J Mater Sci (2009) 44:2882–2889
DOI 10.1007/s10853-009-3381-3

Effects of dynamic strain aging on mechanical properties of SA508 class 3 reactor pressure vessel steel

S. Xu · X. Q. Wu · E. H. Han · W. Ke

Received: 1 December 2008 / Accepted: 3 March 2009 / Published online: 25 March 2009

Abstract An as-received reactor pressure vessel (RPV) steel SA508 class 3 (SA508 Cl.3) has been subjected to uniaxial tension tests in the strain-rate range of 6.67×10^{-5} s^{-1} to 1.2×10^{-2} s^{-1} and the temperature range of 298 K to 673 K to investigate the effects of temperature and strain rate on its mechanical properties. It was found that the region of dynamic strain aging (DSA) was in the temperature range of 523–623 K at a strain rate of 1.2×10^{-3} s^{-1}, 473–573 K at 1.2×10^{-4} s^{-1}, and 473–573 K at 6.67×10^{-5} s^{-1}, respectively. Serrated stress–strain behaviors, predominately consisting of type A, B, and C, have been observed in these temperatures and strain-rate ranges. The solutes responsible for DSA have been identified to be carbon and nitrogen, and nitrogen atoms play a more important role. The relative DSA mechanisms for this RPV steel are discussed.

Introduction

Low-alloy steels have been widely used in pressure boundary components of light water reactor (LWR) in nuclear power plants worldwide. However, it is well known that these types of steels are susceptible to dynamic strain aging (DSA) [1–5]. DSA is a phenomenon of interaction between diffusing solute atoms and mobile dislocations during plastic deformation and usually depends on deformation rate and temperature, which govern the velocity of mobile dislocations and diffusing solute atoms, respectively. The occurrence of DSA can be manifested by the anomalous features of material behavior. While serrated yield is the most commonly observed manifestation of DSA, there are various other concurrent phenomena [6–13]. Other anomalies associated with DSA have been described by Rodriguez [14]: during monotonic tensile deformation, DSA is manifested by the serrated flow in the stress–strain curve, the peak or the plateau in the variation of material strength with temperature, the minima in the variation of ductility with temperature, and the negative strain-rate sensitivity (SRS).

For strength consideration alone, DSA would appear to be a positive attribute of the steel. In addition, fatigue strength and creep strength in the DSA temperature region were reported to be improved by DSA [15, 16]. However, as is often the case, the increased strength is obtained at the cost of decreased ductility and toughness. In fact, it is these latter properties that are commonly emphasized in discussing DSA, as evidenced by the use of the term blue brittleness. The embrittlement associated with this phenomenon may prove detrimental in some applications such as in a large nuclear component, where retention of adequate toughness throughout the service life is of primary importance. The influence of interstitial solutes such as carbon and nitrogen on mechanical and fracture properties of unirradiated reactor pressure vessel (RPV) steels through DSA has been the subject of resent studies [8, 17]. In such a reactor component strain aging can occur in a region of crack-tip plasticity. This would essentially be static since aging that takes place in material already plastically deformed. It may also have a dynamic component in the sense that aging occurs while the plastic zone undergoes a slow deformation during reactor operation. It had been

S. Xu · X. Q. Wu (✉) · E. H. Han · W. Ke
State Key Laboratory for Corrosion and Protection,
Institute of Metal Research, Chinese Academy of Sciences,
62 Wencui Road, Shenyang 110016, People's Republic of China
e-mail: xqwu@imr.ac.cn

S. Xu
e-mail: sxu@imr.ac.cn

reported that an appreciable loss of fracture toughness of some RPV steels at elevated temperature is due to DSA [3, 18, 19]. Li and Leslie [20] have shown that a tensile pre-strain of only 3% at 523 K in a steel susceptible to DSA can cause the ductile-to-brittle fracture transition temperature to increase by as much as 318 K. Wu et al. [21] have found that the presence of hydrogen resulted in a distinct softening in tensile strength and a certain loss in tensile ductility and a remarkable degradation in fatigue crack initiation and propagation resistance in high-temperature water environments in the DSA strain-rate region. In type 316L stainless steel, Hong et al. [22, 23] have also reported DSA reduced the crack initiation and propagation life in air by way of multiple crack initiation, which comes from the DSA-induced inhomogeneity of deformation, and rapid crack propagation due to the DSA-induced hardening, respectively. In nuclear pressure vessel steels, Wu et al. [24–26] believed that DSA has a two-way effect on the fatigue resistance of low-alloy pressure vessel steel in high-temperature water environments. On the one hand, DSA tends to improve the fatigue resistance of the steel by either retarding the crack propagation or improving the steel strength. On the other hand, DSA interacts with surrounding environmental factors and promotes the environmentally assisted cracking (EAC). The above two effects compete with each other in the corrosion fatigue process, and which one is dominant depends on the aggressive degree of the surrounding environments. The typical operating temperature of LWR is 561–618 K which fitly falls in the region of DSA of the RPV steels [27]. Basically these steels cannot be immune from the effects of DSA in their service environments. In order to investigate the influence of DSA on the mechanical properties and the mechanism of DSA interaction with EAC of this steel in their service environments, it must clarify the mechanism of DSA on the mechanical properties at high temperature firstly. However, few systematic investigations were only focused on DSA of this steel; hence, it is of great importance to study the influence of the DSA on mechanical properties of this nuclear structural steel for the structural integrity assessment of the components.

The present study was to investigate the effects of interstitial atoms on mechanical properties of SA508 Cl.3 steel in terms of DSA phenomena, in particular the influence of temperature and strain rate on mechanical properties.

Experimental

The test material was a SA508 Cl.3 forged RPV steel of 250-mm thickness used for the fabrication of PWR reactor pressure vessels, produced by the China First Heavy Industries Co. Ltd. The as-received material had been austenized at 1,163 K for 5 h and water quenched, then tempered at 928 K for 10 h and air cooled, and then followed by simulated post-welding heat treatment at 883–893 K for 30 h and furnace cooled. The chemical composition and heat treatment history are listed in Table 1. The microstructure of the steel was typical upper bainite (Fig. 1). Tensile specimens with a gage section of 5 mm in diameter and 25 mm in length were used in the present study.

To investigate the DSA temperature region of the steel, tensile tests were performed for the as-received materials under a series of temperatures and strain rates. The strain rates were 1.2×10^{-2}, 1.2×10^{-3}, 1.2×10^{-4}, and 6.67×10^{-5} s^{-1}, and test temperature was from 298 K to 673 K.

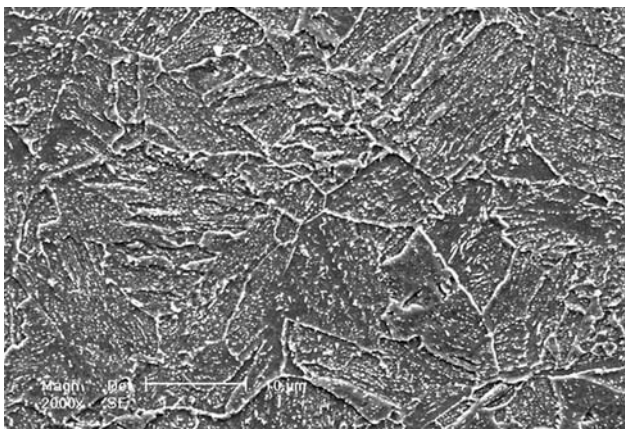

Fig. 1 Optical micrograph of SA508 Cl.3 steel used presently

Table 1 Chemical composition (wt%) and heat treatment of the SA508 Cl.3 pressure vessel steel

C	Si	Mn	P	S	Cr	Ni	Mo	Cu	N	O	Fe
0.185	0.18	1.44	0.005	0.0025	0.13	0.74	0.5	0.02	98.5[a]	17[a]	Bal.

Preliminary heat treatment

Normalizing: 1,203 K (5 h)—air cooling

Tempering: 943 K (14 h)—air cooling

Quality heat treatment

Quenching: 1,163 K (5 h)—water quenching

Tempering: 928 K (10 h)—air cooling

Simulated post-welding heat treatment

883–893 K (30 h)—furnace cooling

[a] ppm

Three specimens were tested for each temperature-strain rate condition. For tests at elevated temperature, three-zone controlled split furnace was used. The specimen was equilibrated for at least 30 min before testing and the temperature control was ~5 °C. The fracture surfaces of the tested specimens were carefully examined using the scanning electron microscope (SEM).

Results

Figure 2 shows some typical segments of tensile stress–strain curves for specimens tested in the temperature range of 298–673 K. At a base strain rate of 1.2×10^{-3} s^{-1}, smooth stress–strain curves were observed at temperature below 473 K and above 673 K; serrated stress–strain curves were observed in the temperature range of 523–623 K (Fig. 2a). At a base temperature of 573 K, smooth stress–strain curves were found at high strain rate of 1.2×10^{-2} s^{-1} and obviously serrated stress–strain were found in the strain rate of 6.67×10^{-5} s^{-1}–1.2×10^{-3} s^{-1} (Fig. 2b). It was found that the height of the serrations increased with increasing temperature (Fig. 2a) and decreased with increasing strain rate (Fig. 2b). These results are generally in agreement with numerous other investigations of DSA [28–30].

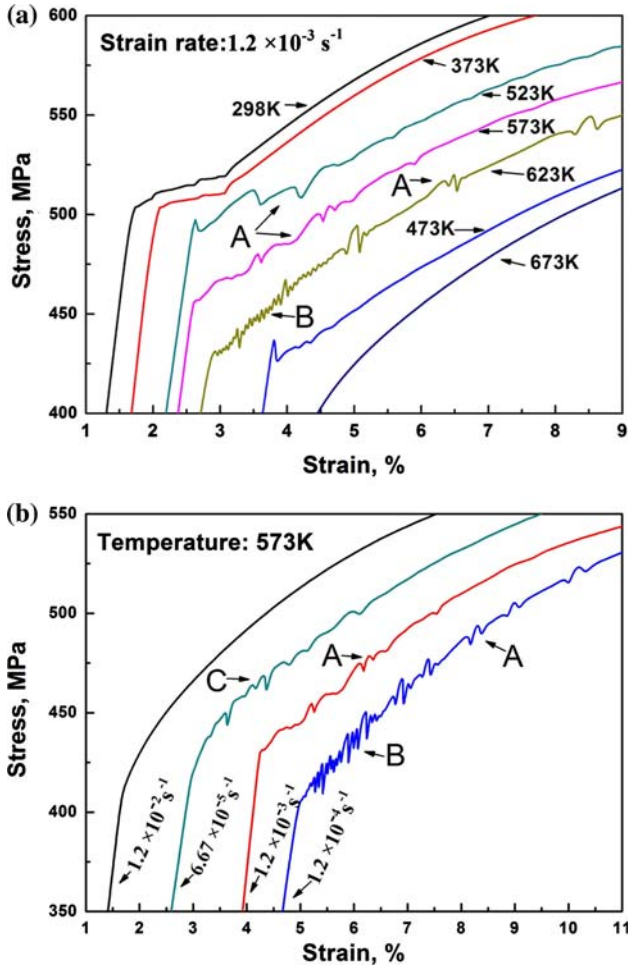

Fig. 2 Some segments of typical stress–strain curves of SA508 Cl.3 steel: **a** temperature: 298–673 K, strain rate: 1.2×10^{-3} s^{-1}; **b** temperature: 573 K, strain rate: 6.67×10^{-5}–1.2×10^{-2} s^{-1}

The above typical serrations could be identified as type A, B, and C according to the generally accepted nomenclature in the literatures [7, 14]. Type A serrations are periodic serrations from repeated deformation bands initiating at the same end and propagating in the same direction. These are locking serrations characterized by an abrupt rise in stress followed by a drop to or below the general level of the stress–strain curve. Type B serrations are oscillations about the general level of the stress–strain curve that occur in quick succession due to discontinuous band propagation arising from the DSA of moving dislocations within the Luders bands. Type C serrations are yield drops below the general level of the stress–strain curve due to unlocking of dislocations.

Figure 3 shows the serration map of this test as a function of temperature and strain rate. At 473 K, only type A serrations were observed. From 523 K to 573 K, type A, B, and C serrations were observed. At 623 K, type A + B serrations were observed. At 673 K, only slight type A serrations were observed at 1.2×10^{-2} s^{-1}. At the slowest strain rate, i.e., 6.67×10^{-5} s^{-1}, type C serration was observed at temperature 573 K (Fig. 2b). At the intermediate strain rate, i.e., 1.2×10^{-3} s^{-1} and 1.2×10^{-4} s^{-1}, type A and A + B were observed in the temperature range of 473–623 K (Fig. 2a and b). At the fastest strain rate, i.e., 1.2×10^{-2} s^{-1}, only small type A serration was found at 673 K. The type A serrations occurring in the temperature range of 473–673 K became scarce with progressive

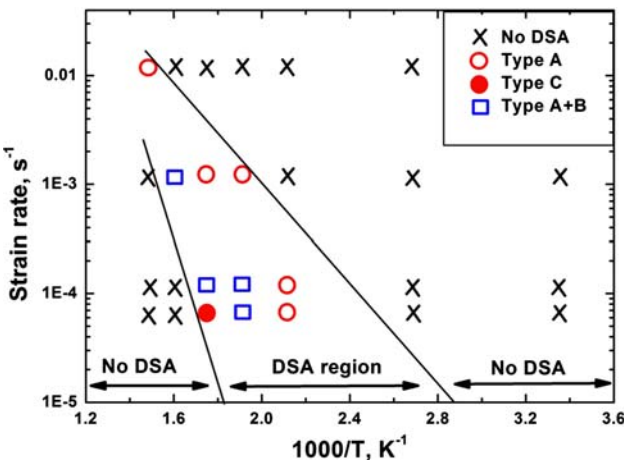

Fig. 3 Summary of observations made on serrated flow behavior in alloy SA508 Cl.3

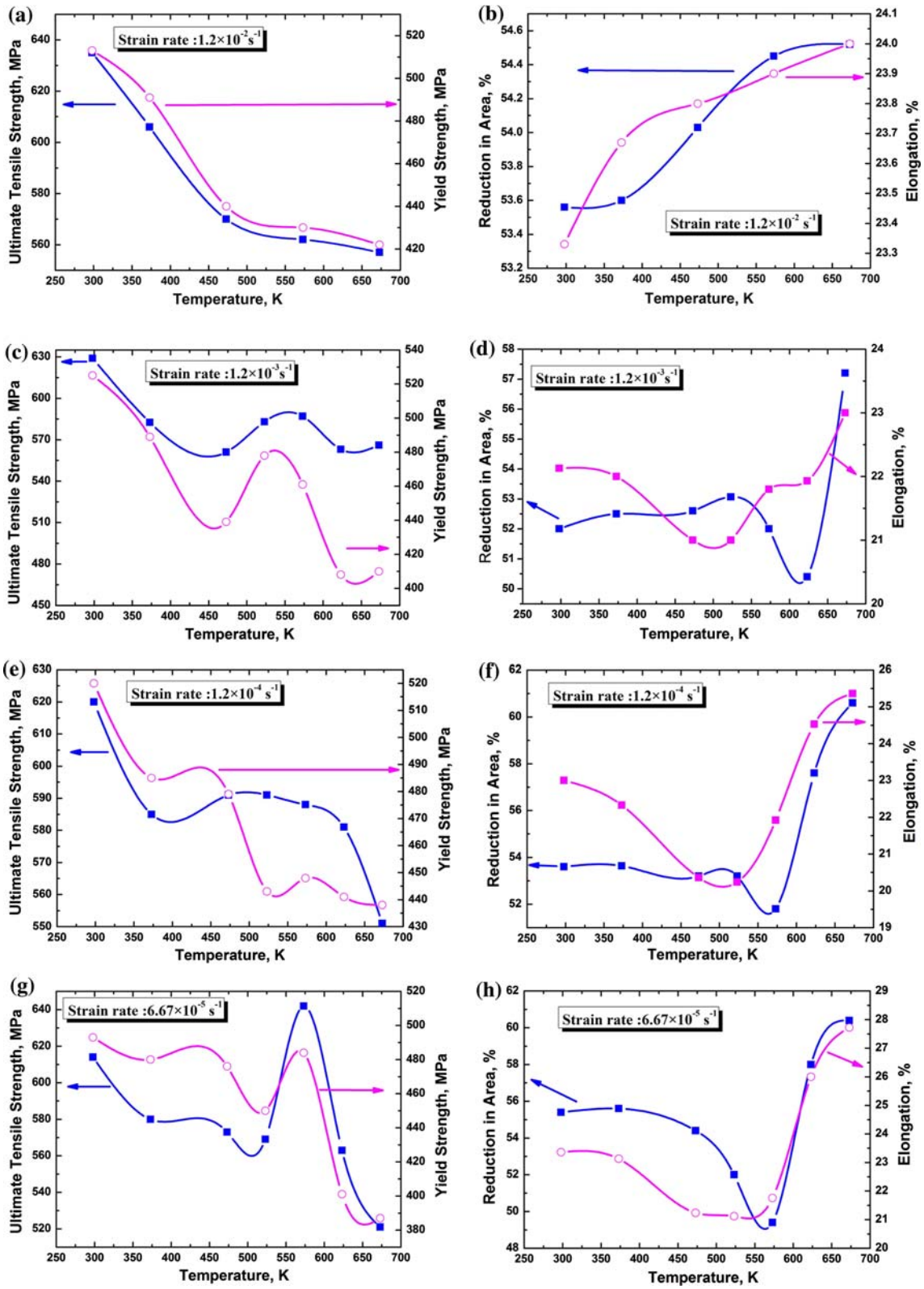

Fig. 4 Temperature dependence of yield strength, ultimate tensile strength, uniform elongation, and reduction of the area at various strain rates: **a** and **b** 1.2×10^{-2} s^{-1}; **c** and **d** 1.2×10^{-3} s^{-1}; **e** and **f** 1.2×10^{-4} s^{-1}; and **g** and **h** 6.67×10^{-5} s^{-1}

deformation and generally disappeared at larger strains. In the temperature range of 523–623 K, mixture of type A + B serrations was observed (Fig. 2a), and type B serrations occurred at small strain and type A serrations occurred at large strain (Fig. 2b).

Figure 4 shows dependence of temperature on tensile properties (yield strength, ultimate tensile strength, elongation, and reduction in area) of SA508 Cl.3 steel. At the strain rate of 1.2×10^{-2} s^{-1}, the yield strength and ultimate tensile strength decreased with increasing temperature, and the elongation and reduction in area increased with increasing temperature. At the strain rate of 1.2×10^{-3} s^{-1}, the yield strength and ultimate tensile strength decreased with increasing temperatures up to 473 K, and then gradually increased between the temperature 523 K and 623 K. Further, a minimum elongation and a peak reduction in area appeared in the temperature range of 523–623 K, which is a typical DSA phenomenon. Similarly, at the strain rate of 1.2×10^{-4} s^{-1}, the DSA temperature region was between 473 K and 573 K; at the strain rate of 6.67×10^{-5} s^{-1}, the DSA temperature region is also between 473 K and 573 K.

Figure 5 shows the high-magnification morphologies of SA508 Cl.3 steel at four testing temperatures. The fracture modes of the tested specimens were essentially ductile and the fracture occurred predominantly by micro-void coalescence. The preferred nucleation sites for dimples were between the closely spaced carbides or at the intersection of multiple laths as indicated by the longitudinal section morphology adjacent to the necked zone (Fig. 5). At room temperature, some featureless flat, or brittle-like areas, appeared on the fracture surfaces (Fig. 5a). Moreover, a few volcano-like areas were observed around the large inclusions on the fracture surfaces. The surfaces of these volcanoes and the adjacent areas appeared relatively smooth or quasi-cleavage-like patterns (Fig. 5b and c). The results are in good agreement with the increase of tensile strength, but the loss of fracture toughness induced by DSA. In addition, the dimples formed at DSA temperatures (Fig. 5c) became shallower than those at the room temperature (Fig. 5a), coinciding with the literature's results [18, 31].

Discussion

Tensile tests of the present SA508 Cl.3 steel clearly indicated the occurrence of DSA. It was observed that the critical temperature for the appearance and disappearance of serrated flow depended on the applied strain rate, which was a typical indication of DSA. Three types of DSA have been found in wide range of temperatures and strain rates, namely, type A, B, and C. The main factors influencing the type of the DSA were found to be imposed strain rate and testing temperature. When the strain rate decreases (waiting time of dislocations increases) or the temperature increases (mobility of solute increases), the DSA evolves from type A to type B and to type C (Fig. 3). The underlying mechanisms could be described as follows. In the case of high strain rate (type A), diffusion of solute atoms to arrested dislocations has less time to complete, hence obstacles to dislocation break-away are looser. Further, little time is allowed for the plastic relaxation of the long-range elastic

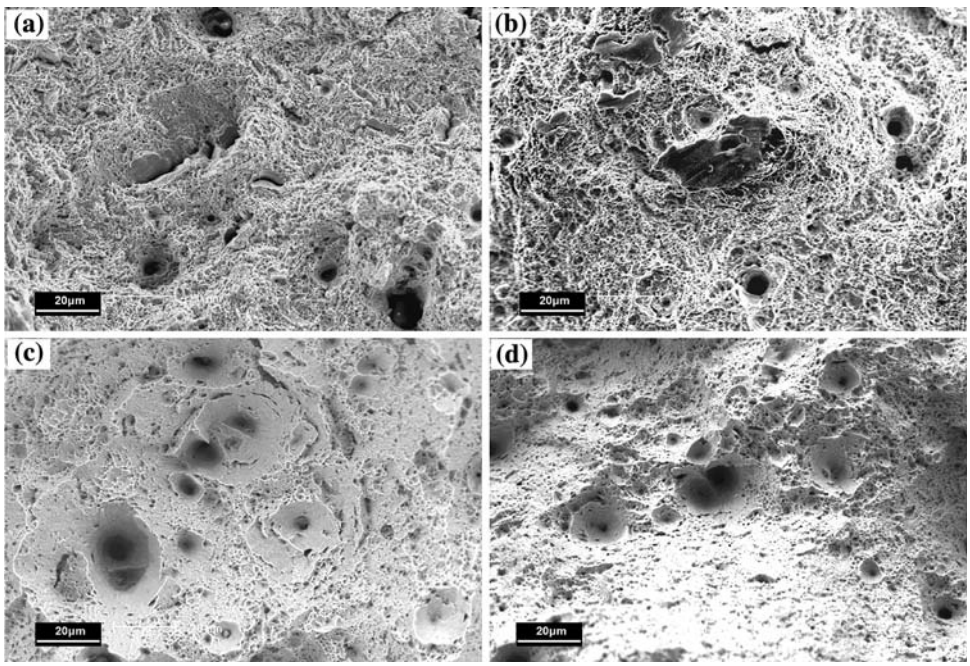

Fig. 5 SEM for the high-magnification fracture surface from tensile tests at the strain rate of 1.2×10^{-4} s^{-1} and at four tested temperatures: **a** 298 K; **b** 523 K; **c** 573 K; and **d** 673 K

internal stresses stemming from strain incompatibility in the band area. As a result, the periodic serrations were observed [32]. In the case of intermediate strain rate (type B), obstacles to dislocation break-away are stronger, due to additional solute diffusion time, whereas spatial correlations due to elastic internal stresses are weaker, due to their plastic relaxation during longer reloading times. Hence, a larger fraction of dislocation ensembles remains in the pinned state, spreading of plastic activity is limited and unlocking events are more typical in size. Similar conjectures were previously presented in the literatures [32–34]. In the case of low strain rate (type C), the critical strain increases with an increase in temperature and or with a decrease in strain rate. This is also referred to as inverse DSA phenomenon. Understanding and modeling of type C serrations remains incomplete. One of the early models [35] suggests that in this domain the diffusion rates are sufficiently large for the dislocations to be aged even at low strains and the unlocking type C serrations occur due to the breakaway of these aged dislocations. It has also been suggested that type C serrations are associated with draining of solutes by precipitation [36].

Many theoretical models have been put forward to explain DSA [9, 11, 13]. Various investigations on serrated flow suggest that the measurement of the critical strain for the onset of serrations, ε_c, and its dependence on strain rate and temperature are essential to understand the underlying mechanisms. This dependence is generally expressed as

$$\varepsilon_c^{(m+\beta)} = K\dot{\varepsilon}\exp(Q/kT) \quad (1)$$

where m and β are the respective exponents in the relations for the variation of vacancy concentration (C_v) and mobile dislocation density (ρ_m) with plastic strain, $\rho_m \propto \varepsilon^{\beta}$ $C_v \propto \varepsilon^m$, K is a constant, $\dot{\varepsilon}$ is the strain rate, Q is the activation energy, k is the Boltzman constant, and T is the absolute temperature [11, 14]. The exponent $(m + \beta)$ can be obtained as the slope on the plot of ln(*strain rate*) versus ln ε_c at a constant temperature, as shown in Fig. 6. The value of the exponent $(m + \beta)$ is listed in Table 2. It is clear that the critical strain for the onset of serrations, ε_c increased with the stain rate. The slope of this plot yielded the value of $(m + \beta)$ in the range of 1.176–1.325, and the average value was 1.26. The parameter $(m + \beta)$ is often used to identify the mechanism involved in serrated flow [14, 37]. It is proposed that when $m + \beta$ is close to unity, interstitial solutes are responsible for strain aging; when $m + \beta$ is in the range of 2–3, substitution solutes are responsible for strain aging. Our experiment results, therefore, indicated that interstitial atoms could be responsible for the observed serrated flow.

The mechanism of DSA can be identified by evaluating the activation energy for DSA and comparing them with those reported in the literatures because DSA is a thermally activated process associated with interaction between

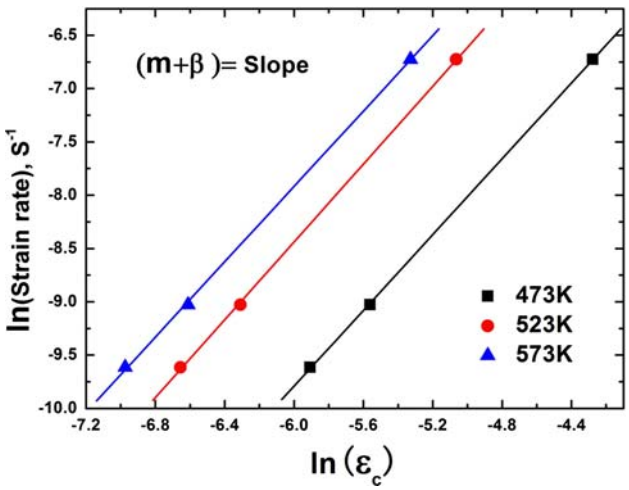

Fig. 6 Plot of ln(*strain rate*) versus ln ε_c used to obtain $(m + \beta)$ at different temperature

Table 2 $(m + \beta)$ and Q values obtained from the Figs. 6 and 7

T (K)	473	523	573
$m + \beta$	1.272	1.325	1.176
Average $(m + \beta)$	1.26		
Strain rate (s^{-1})	1.2×10^{-3}	1.2×10^{-4}	6.67×10^{-5}
Q (kJ/mol)	89.2	86.7	94.0
Average Q	89.97		

diffusing solute atoms and mobile dislocations. There are several methods for evaluating Q associated with the serrated flow. Following Eq. 1, Q can be calculated according to the slope of a plot of lnε_c versus $1/T$ at a constant strain rate as follows.

$$Q = \text{slope} \times (m + \beta) \times k \quad (2)$$

However, as pointed out by Qian and Reed-Hill [38], this method involves the use of an average value of $(m + \beta)$ obtained over a range of temperatures. Sleeswyk [39] suggested an alternative strain aging model that was later modified by McCormick [11]. In this model called "static strain aging", aging of the dislocations occurs while they wait at obstacles. By equating the waiting time at obstacles with the aging time the following equation is obtained.

$$\varepsilon_c^{(m+\beta)} \Big/ T = \left(\frac{C_1}{\phi C_0}\right)^{3/2} \frac{kb}{LNU_m} \frac{\exp(Q/kT)}{D_0}\dot{\varepsilon} \quad (3)$$

where C_0 is the initial concentration of solute in the alloy, C_1 is the local concentration of the solute at the dislocation, L is the obstacle spacing, U_m is the maximum solute-dislocation interaction energy, D_0 is the frequency factor, b is the Burger's vector, and N and ϕ are constants. This method has been employed to identify the elements responsible for serrated flow by determining activation

energy for a large number of alloy systems [38, 40]. Q can be evaluated for a given value from the plot of $\ln \varepsilon_c^{(m+\beta)}/T$ versus $1/T$ as $Q = \text{slope} \times k$. In this method, it would be possible to use the individual values of $(m + \beta)$ obtained at different temperatures. The value of $(m + \beta)$ from the Fig. 6 is used to calculate the activation energy for the onset of serration from the slope of the plot of $\ln \varepsilon_c^{(m+\beta)}/T$ versus $1/T$ (Fig. 7). The values of the activation energy at different strain rates are listed in Table 2.

In the present work, activation energies for the onset of serrations were determined in the range of 86.7–94 kJ mol^{-1}, which are close to the activation energies for lattice diffusion of carbon and nitrogen in α-iron alloys (the activation energies of carbon and nitrogen are 76.7 kJ mol^{-1} and 82.0 kJ mol^{-1} in α-iron alloys, respectively [18].). This result agreed well with the result of Kang et al. [18] who obtained the activation energy of 90.6 kJ mol^{-1} for a SA508 Cl.3 steel. Baird and Jamieson [1] also obtained activation energy of 63–84 kJ mol^{-1} for Fe–N alloy. Nakada and Keh [41] noted that although the measured activation energy was not affected by the chemical composition of the steels and Fe alloy, the temperature and strain rates at which serrations occurred were strongly dependent upon the concentration of carbon plus nitrogen. Although the carbon is hardly soluble in α-Fe showing the smaller solubility-a factor of 100 less than that of nitrogen among the bcc metals, and the carbon diffusive behavior inside the lattice is strongly related to the energy gradients linking the different available sites, eventually to the interaction with lattice defects. However, this approach may be the case for temperature below approximately 373 K, at higher temperature the increased solubility of carbon can cause strain aging even in the absence of nitrogen [4]. Thus, when two elements are present, both of them can contribute to strain aging at temperatures above about 373 K. In the present study, it is believed that the DSA

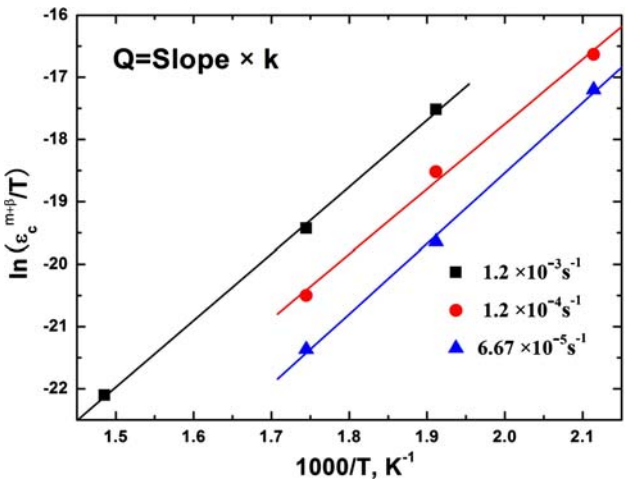

Fig. 7 Representative plot of $\ln \varepsilon_c^{(m+\beta)}/T$ versus $1/T$ used to determine Q at different stain rate

phenomenon is primarily due to nitrogen element. On the one hand, most of carbon atoms have been precipitated in the form of Fe_3C leaving a few of carbon atoms in solution state at room temperature (Fig. 1). On the other hand, up to about 523 K a large number of nitrogen atoms (in some cases, about 10 times) remain as interstitial solutes compared to carbon atoms [42]. Therefore, the experimental conditions (temperatures and strain rates) under which serrated flow is observed are critically influenced by the available interstitial atoms in solution state, in particular nitrogen. In addition, the amount of dissolved nitrogen needed to cause some evidence of strain aging is extremely small (only 0.0004 wt%) [4]. Nitrogen atoms have more significant influence on DSA because of their higher solubility and mobility compared to carbon atoms.

Conclusions

Dynamic strain aging has been observed for as-received SA508 Cl.3 RPV steel within a certain range of temperatures and strain rates during tensile deformation. The region of DSA was in the temperature range of 523–623 K at a strain rate of 1.2×10^{-3} s^{-1}, 473–573 K at 1.2×10^{-4} s^{-1}, and 473–573 K at 6.67×10^{-5} s^{-1}, respectively. Typical serrated stress–strain curves have been observed in DSA regime. Type A serrations were observed in the whole DSA temperature range (473–673 K). Type (A + B) serrations were observed in the middle temperatures range (523–623 K), whereas type C serrations appeared at 573 K. In DSA region, a sharp increase in ultimate tensile strength, yield strength, and a moderate reduction in ductility have been observed. Calculated $m + \beta$ values were in the range of 1.176–1.325, suggesting that interaction of interstitial atoms with moving dislocations is responsible for the observed serrations. Activation energy for serrated flow was calculated to be 86.7–94 kJ mol^{-1}. It is believed that carbon and nitrogen atoms were responsible for the DSA in the present study. Nitrogen atoms may play a more important role on DSA because of their higher solubility and mobility compared to carbon atoms.

Acknowledgements The authors would like to thank Prof. R. S. Chen, Dr. S. M. Liang, W. N. Tang, and L. Gao for their help on the tensile experiments. This study was jointly supported by the Special Funds for the Major State Basic Research Projects (2006CB605005) and the innovation fund of IMR, CAS.

References

1. Baird JD, Jamieson A (1966) J Iron Steel Inst 204:793
2. Kang SS, Kim IS (1992) Nucl Technol 97:336
3. Kim IS, Kang SS (1995) Int J Pres Ves Piping 62:123
4. Leslie WC, Rickett RL (1983) Trans AIME 10:21

5. Wagner D, Moreno JC, Prioul C, Frund JM, Houssin B (2002) J Nucl Mater 300:178
6. Blakemore JS, Hall EO (1966) J Iron Steel Inst 204:817
7. Brindley BJ, Barnby JT (1966) Acta Metall 14:1965
8. Chakravartty JK, Wadekar SL, Sinha TK, Asundi MK (1983) J Nucl Mater 119:51
9. Cottrell AH (1953) Phil Mag 44:829
10. Kubin LP, Estrin Y (1991) J Phys III 1:929
11. McCormick PG (1972) Acta Metall 20:351
12. Mulford RA, Kocks UF (1979) Acta Metall 27:1125
13. Wilson DV (1973) Acta Metall 21:373
14. Rodriguez P (1984) Bull Mater Sci 6:653
15. Baird JD (1971) Met Rev 16:1
16. Tsuzaki K, Matsuzaki Y, Maki T, Tamura I (1991) Mater Sci Eng A 142:63
17. Mohan R, Marschall C (1998) Acta Mater 46(6):1933
18. Kang SS (1994) PhD thesis, Advance Institute of Science and Technology, Korea
19. Kim KC, Kim JT, Suk JI, Sung UH, Kwon HK (2004) Nucl Eng Des 228:151
20. Li CC, Leslie WC (1978) Metall Trans 9A:1765
21. Wu XQ, Katada Y, Lee SG, Kim IS (2004) Metall Mater Trans 35A:1477
22. Hong SG, Lee SB (2004) J Nucl Mater 328:232
23. Hong SG, Lee SB (2005) J Nucl Mater 340:307
24. Wu XQ, Katada Y (2005) J Mater Sci 40:1953. doi:10.1007/s10853-005-1216-4
25. Wu XQ, Katada Y (2007) J Mater Sci 42:633. doi:10.1007/s10853-006-1144-y
26. Wu XQ, Katada Y (2004) J Nucl Mater 328:115
27. Scott PM (1985) Corros Sci 25(8/9):583
28. Gupta C, Chakravartty JK, Wadekar SL, Dubey JS (2000) Mater Sci Eng A 292:49
29. Hale CL, Rollings WS, Weaver ML (2001) Mater Sci Eng A 300:153
30. Shankar V, Valsan M, Bhanu K, Rao S, Mannan SL (2004) Metall Mater Trans 35A:3129
31. Wu XQ, Kim IS (2003) Mater Sci Eng A 348:309
32. Kok S, Bharathi MS, Beaudoin AJ, Fressengeas C, Ananthakrishna G, Kubin LP, Lebyodkin M (2003) Acta Mater 51:3651
33. Ananthakrishna G, Bharathi MS (2004) Phys Rev E 70:26
34. Ananthakrishna G, Fressengeas C (2005) Scripta Mater 52:425
35. Charnock W (1969) Phil Mag 20:427
36. Kubin LP, Estrin Y (1990) Acta Metall 38:697
37. Rodriguez P, Venkadesan S (1995) Key Eng Mater 103:257
38. Qian KW, Reed-Hill RE (1983) Acta Metall 31:87
39. Sleeswyk AW (1958) Acta Metall 6:598
40. Kim IS, Chaturvedi M (1979) Mater Sci 12:691
41. Nakada Y, Keh AS (1970) Acta Metall 18:437
42. Hall EO (1952) J Iron Steel Inst 10:331